

Millimetre-waves to Terahertz SISO and MIMO Continuous Variable Quantum Key Distribution

Mingqi Zhang¹, Stefano Pirandola², and Kaveh Delfanazari^{1,*}

¹ *Electronics and Nanoscale Engineering Division, James Watt School of Engineering, University of Glasgow, Glasgow G12 8QQ, UK*

² *Department of Computer Science, University of York, York YO10 5GH, UK*

*Corresponding author: kaveh.delfanazari@glasgow.ac.uk

Dated:25122022

Abstract—With the exponentially increased demands for large bandwidth, it is important to think about the best network platform as well as the security and privacy of the information in communication networks. Millimetre (mm)-waves and terahertz (THz) with high carrier frequency are proposed as the enabling technologies to overcome Shannon’s channel capacity limit of existing communication systems by providing ultrawide bandwidth signals. Mm-waves and THz are also able to build wireless links compatible with optical communication systems. However, most solid-state components that can operate reasonably efficiently at these frequency ranges (100GHz-10THz), especially sources and detectors, require cryogenic cooling, as is a requirement for most quantum systems. Here, we show that secure mm-waves and THz QKD can be achieved when the sources and detectors operate at cryogenic temperatures down to $T=4\text{K}$. We compare single-input single-output (SISO) and multiple-input multiple-output (MIMO) Continuous Variable THz Quantum Key Distribution (CVQKD) schemes and find the positive secret key rate in the frequency ranges between $f=100\text{GHz}$ and 1THz . Moreover, we find that the maximum transmission distance could be extended, the secret key rate could be improved in lower temperatures, and achieve a maximum secure communication distance of more than 5Km at $f=100\text{GHz}$ and $T=4\text{K}$ by using 1024×1024 antennas. Our results may contribute to the efforts to develop next-generation secure wireless communication systems and quantum internet for applications from inter-satellite and deep space, to indoor and short-distance communications.

Index Terms— Millimetre (mm)-waves, terahertz (THz) waves, 6G communication, quantum key distribution (QKD), quantum communication, cryogenic system, MIMO, SISO,

I. INTRODUCTION

With the extension of wireless communication and the fast development of information security, higher carrier frequencies and more spectral resources are required [1, 2]. Millimetre (mm)- and terahertz (THz)- waves [3-6] offer ultrawide bandwidth and high-speed data rate communication and are considered to build next-generation (6G) communication systems [7-11]. Mm-waves and THz bands lie between the mature microwave and optical bands as less explored area [12-16]. A gap in the electromagnetic spectrum exists at these

frequency ranges due to the inefficient and unpractical of the devices and circuit [1-19]. However, the recent development of electronic, photonic and plasmonic-based mm-waves and THz technologies help close this gap with the demonstration of power-efficient sources [20-26], antennas [27-31], filters [32-34], waveguides [29, 35-39], modulators [40-49], and detectors [3, 49-52]. Demands for 6G are including, but are not limited to, Terabit per second (Tb/s), mm-precision sensing and positioning, seamless connectivity, and ultrafast wireless communications [7-11]. Moreover, practical implementation of quantum processors and quantum computers operating at low temperatures (cryogenics) [53-55], requires massive open air and free space data transfer from and to high-performance classical processors, computers, and communication systems. Therefore, to realise a robust building block for practical quantum information processing attention should be on both security and low-temperature operation. Compared with the free-space optical link, the THz link is more stable under harsh environments such as fog conditions [56]. The limit of mm-waves [57] and THz links [58, 59] in long distances is mainly caused by the absorption of the air [60]. So it is important to find the window with low atmospheric absorption through this band. High-level security is also an important aspect of realising mm-waves and THz communications which is quite challenging to maintain with classical cryptography schemes. Quantum key distribution (QKD) can help to achieve the goal of high-level unconditional security with the power of the quantum physics [61-64]. QKD could be divided into discrete variables (DVQKD based on single photon sources and detectors) and continuous variables (CVQKD based on standard communication systems) [62-75]. CVQKD uses coherent homodyne detection instead of single photon detection [65] and could be integrated with next-generation communication systems [66].

Single-input single-output (SISO) is a kind of classical communication system where the transmitter and receiver don’t have several antennas. To meet the explosion of data transmission, multiple-input multiple-output (MIMO) technology has been widely used in wireless communication nowadays. MIMO system with multiple antennas at both the transmitter and receiver side brings benefits on data throughput and communication range with limited bandwidth and transmit power [67]. THz QKD with SISO and MIMO systems was introduced in Refs [61] and [68], with the main focus on mid-

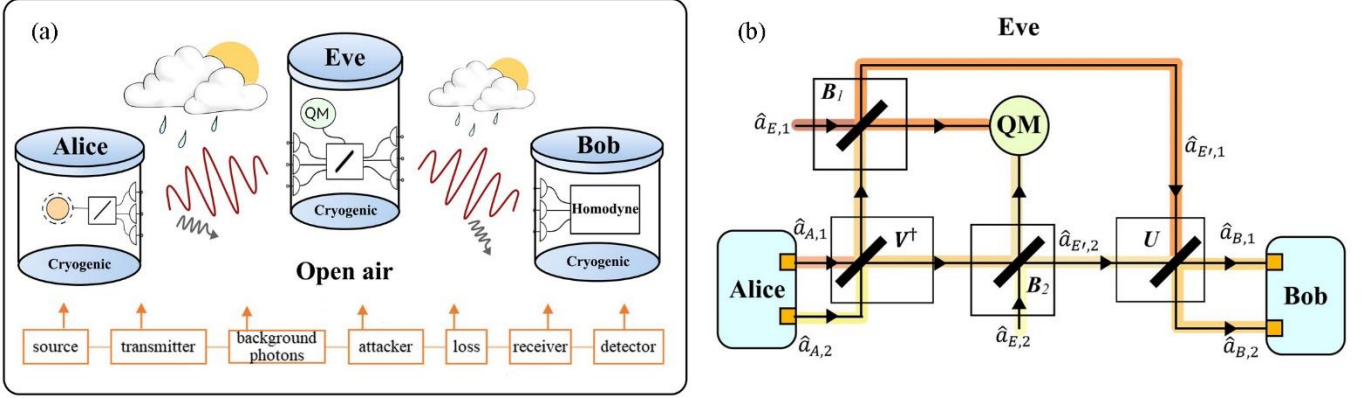


Fig. 1. (a) The system model of the proposed mm-waves and THz QKD. Alice prepares thermal states at the source which denotes a generator. The transmitter and receiver are antennas distributed in a one-dimensional uniform linear array (ULA). Alice, Bob, and Eve do their job at cryogenic ambient (low temperature). The channel loss through the open-air environment contains atmospheric absorption and free-space loss. Eve's output modes are stored in a quantum memory (QM). Bob uses a homodyne detector to measure quadrature. (b) The schematic of the phase shifters model described for a 2×2 MIMO system. The channel is modelled by 4 beam splitters. Alice generates 2 coherent states $\hat{a}_{A,1}$ and $\hat{a}_{A,2}$ based on random vectors and send them out from her 2 antennas as thermal states. These two states are mixed by the first beam-splitter V^\dagger . Then Eve operates collective Gaussian attack. She prepares two two-mode squeezed vacuum states and uses beam-splitter B_1 and B_2 to combine the input and her states. The output and one of the original modes are saved in quantum memory (QM). Before Bob detects the input, the signals are mixed by beam-splitter U . At last, Bob uses his two antennas to receive the modes $\hat{a}_{B,1}$ and $\hat{a}_{B,2}$.

and far-infrared frequency ranges (10THz-40THz) at room temperature ($T=296$ K).

Motivated by the works of [61] and [68], this work focuses on SISO and MIMO QKD at the temperature of $T < 50$ K. We investigate CVQKD at frequency ranges of mm-waves and THz, from $f=100$ GHz to 1 THz, with antennas and detectors both operating in the cryogenic environment ($T < 50$ K). Moreover, we compare the performance of both the SISO and MIMO CVQKD systems at this frequency range.

II. SYSTEM MODEL

For the proposed mm-waves and THz quantum communication scheme, the cryogenic antennas generate electromagnetic (EM) fields that oscillate at an angular frequency ω . This EM field is quantized and the system gets a Hamiltonian $H = \hbar\omega(\hat{a}^\dagger\hat{a} + \frac{1}{2})$. The H is similar to the Hamiltonian of a quantum harmonic oscillator with \hbar as Planck's constant, \hat{a} as the annihilation operator, and \hat{a}^\dagger as the creation operator. Moreover, the quadrature field operators $\hat{q} = \frac{\hat{a} + \hat{a}^\dagger}{\sqrt{2}}$ and $\hat{p} = \frac{i(\hat{a} - \hat{a}^\dagger)}{\sqrt{2}}$ are dimensionless canonical observables of the system (similar to the position and momentum of the quantum harmonic oscillator) [69]. Finally, coherent states of the system are the eigenstates of the annihilation operator \hat{a} , provided by $\hat{a}|\alpha\rangle = \alpha|\alpha\rangle$. Here, $\alpha = q + ip \in \mathbb{C}$ indicates the coherent state amplitude [68], taken from a two-dimensional Gaussian distribution. Two independent continuous variables q and p are used to create a secret key between Alice and Bob [61].

Notation: Boldface and italic capital letters such as \mathbf{A} denote matrices. \mathbf{A}^\dagger is the conjugate transpose of matrix \mathbf{A} while \mathbf{A}^T is the transpose. $\mathbf{0}_{M \times N} \in \mathbb{C}^{M \times N}$ is a zero complex matrix and

$\mathbf{1}_{M \times N} \in \mathbb{C}^{M \times N}$ is a complex matrix of ones. \mathbf{I}_M represents a $M \times M$ identity matrix. A $M \times M$ diagonal matrix described by $\text{diag}(\mathbf{a})$ with $\mathbf{a} \in \mathbb{C}^M$ shows \mathbf{a} on its diagonal. And $\mathcal{N}(\mu, \Sigma)$ is a real multivariate Gaussian distribution in which the vector is μ and the covariance matrix (CM) is Σ .

A. Channel model

We consider a one-way communication channel to build a secret key between Alice and Bob as shown in Fig.1 (a). A MIMO mm-waves and THz communication channel between Alice and Bob include a transmitter with N_t antennas at Alice's side and a receiver with N_r antennas at Bob's side. We assume the antennas at both sides are distributed in a one-dimensional uniform linear array (ULA) with each antenna element's gain G_a . So the antenna gains of Alice and Bob are $G_t = N_t G_a$ and $G_r = N_r G_a$ [68]. The Gaussian modulation of the thermal state is a widely used encoding protocol for several frequencies [61]. Alice begins with a vacuum state $|0\rangle$ and generates N_t coherent states $|\alpha_i\rangle$ with amplitudes $\alpha_i = Q_{A,i} + jP_{A,i}$, $i = 1, 2, \dots, N_t$ from the N_t antennas with quadratures being chosen from two independent random vectors $\mathbf{Q}, \mathbf{P} \sim \mathcal{N}(\mathbf{0}_{N_t \times 1}, V_s \mathbf{I}_{N_t})$ where V_s is the variance of the initial signal encoding [68]. Two quadratures $\hat{Q}_{A,i}$ and $\hat{P}_{A,i}$ of a quantum THz source (thermal) state are randomly sent by the i -th antenna element of Alice and described by $\hat{X}_{A,i} \in \{\hat{Q}_{A,i}, \hat{P}_{A,i}\}$. So the i -th mode of Alice can be considered as $\hat{X}_{A,i} = \alpha_i + \hat{0}$, where $\hat{0}$ is the thermal mode (quadrature operator) due to the background thermal noise at mm-waves and THz and $X_{A,i}$ denotes the classical modulated variable [61, 76]. The total variance of Alice's mode is

$$V_a = V_s + V_0 \quad (1)$$

where V_0 is the variance of thermal state (contains variance of vacuum mode and variance of preparation noise) [61]. V_0 is defined as

$$V_0 = 1 + 2\bar{n} \quad (2)$$

Here, 1 is the vacuum shot noise unit (SNU) and

$$\bar{n} = \left[\exp\left(\frac{hf_c}{k_B T}\right) - 1 \right]^{-1} \quad (3)$$

is the mean thermal photon number, h is Planck's constant, k_B denotes Boltzmann's constant, T is the environment temperature, and f_c is the carrier frequency. Now, let's consider Alice sends her states to Bob (receiver) over an insecure quantum channel. Bob uses a noisy homodyne detection technique, which is based on mm-waves and THz shot-noise limited quantum detector that randomly switches between quadrature \hat{Q} and \hat{P} , to measure the incoming thermal states.

The channel matrix between Alice and Bob could be modelled as [68, 70, 71]

$$\mathbf{H} = \sum_{l=1}^L \sqrt{\gamma_l} e^{j2\pi f_c \tau_l} \psi_{N_r}(\phi_{r,LOS}) \psi_{N_t}^\dagger(\phi_{t,LOS}) \quad (4)$$

where, $\mathbf{H} \in \mathbb{C}^{N_r \times N_t}$, L is the full number of multipath components, τ_l is the propagation delay of the l -th multipath. We only consider the line-of-sight (LOS) path with $L=1$ in this work. So the path loss γ_l is given by [68]

$$\gamma_{l=1} = G_t G_r \left(\frac{\lambda}{4\pi d}\right)^2 10^{-\frac{\delta d}{10}} \quad (5)$$

where d is the distance (km) between Alice and Bob and δ is the atmospheric loss and is defined as dB/km [61, 70]. It contains both the free space path and the atmospheric absorption losses of mm-waves and THz waves. $\phi_{r,LOS}$ and $\phi_{t,LOS}$ is the angle of arrival seen by Bob, and the angle of departure from Alice, respectively. $\psi_K(\theta)$ represents the array response vector of a ULA which contains K number of antennas.

The derivation details of the channel model are described by a singular-value decomposition (SVD) scheme introduced by Ref. [68] are presented in Appendix A.

Although the coherent attack is the general attack, the works reported in Refs. [72, 73] proved that once the system is secure against collective attacks, it is also secure against general attacks with the long secret key. In CVQKD, the most realistic and studied collective attack against Gaussian protocols is the entangling cloner attack [61]. So, we assume the channel are totally under Eve's control and she uses entangling cloners to steal information. Fig.1 (b) shows a 2×2 MIMO system built by 4 beam-splitters as an example [69]. After the two transmitted modes from Alice are combined by beam-splitter \mathbf{V}^\dagger , Eve will pick up two produced output modes. Eve should prepare two pairs of entangled Einstein-Podolsky-Rosen $\{\hat{e}_1, \hat{E}_1\}$ and $\{\hat{e}_2, \hat{E}_2\}$ (known also as two-mode squeezed vacuum states) in advance. Once received the input, Eve uses \mathbf{B}_1 and \mathbf{B}_2 to combine them with \hat{E}_1 and \hat{E}_2 . The relationship of input and output of \mathbf{B}_i can be written as [68, 69]

$$\begin{bmatrix} \hat{a}_{out,1} \\ \hat{a}_{out,2} \end{bmatrix} = \begin{bmatrix} \sqrt{\eta_i} & \sqrt{1-\eta_i} \\ -\sqrt{1-\eta_i} & \sqrt{\eta_i} \end{bmatrix} \begin{bmatrix} \hat{a}_{in,1} \\ \hat{a}_{in,2} \end{bmatrix} \quad (6)$$

Here, η_i is the round trip transmissivity of two port beam-splitter \mathbf{B}_i . Then Eve will save one of the outputs from every beam-splitters (\hat{E}'_1, \hat{E}'_2) and the original modes (\hat{e}_1, \hat{e}_2) in her quantum memory (QM) and measure the ancilla modes to exploit information when Alice and Bob completed their classical communication. The other two output modes will be

combined by the beam-splitter \mathbf{U} and sent to Bob. We assume Alice applies \mathbf{V} as the base of beamforming at her end, and Bob employs \mathbf{U}^\dagger as the base of decoding at his side. The whole model could be described by [68, 69]

$$\hat{\mathbf{a}}_B = \mathbf{U}^\dagger \mathbf{H} \mathbf{V} \hat{\mathbf{a}}_A + \mathbf{U}^\dagger \mathbf{U} \mathbf{S} \hat{\mathbf{a}}_E \quad (7)$$

where $\hat{\mathbf{a}}_B = [\hat{a}_{B,1}, \dots, \hat{a}_{B,N_r}]^T$ is the received mode of Bob, $\hat{\mathbf{a}}_A = [\hat{a}_{A,1}, \dots, \hat{a}_{A,N_t}]^T$ is the transmitted mode of Alice, $\hat{\mathbf{a}}_E = [\hat{a}_{E,1}, \dots, \hat{a}_{E,N_t}]^T$ is the injected Gaussian mode of Eve.

$$\mathbf{S} = \text{diag}\{\sqrt{1-\eta_1}, \dots, \sqrt{1-\eta_r}, \mathbf{1}_{(M-r) \times 1}\} \quad (8)$$

is a diagonal matrix with $M = \min(N_t, N_r)$. The calculation details could be found in Appendix A. The efficient channel between Alice and Bob can be disintegrated into r parallel SISO channels by utilizing the SVD of \mathbf{H} (r is the rank of \mathbf{H}). In this case, the relation between channels' input and output can be written as [68]

$$\hat{\mathbf{a}}_{B,i} = \sqrt{T_i} \hat{\mathbf{a}}_{A,i} + \sqrt{1-T_i} \hat{\mathbf{a}}_{E,i}, \quad i = 1, 2, \dots, r \quad (9)$$

Here, T_i is the i -th non-zero eigenvalue of $\mathbf{H}^\dagger \mathbf{H}$ and could also be considered as the i -th transmissivity of the channel. Homodyne experiments on one of the randomly selected quadratures will be performed by Bob for every r -received mode and get the result detailed in Appendix A.

We set W to the variance of the thermal noise introduced by Eve. So, Bob will receive the i -th mode with the shot-noise level $V(\hat{X}_{B,i}) = T_i V_0 + (1-T_i)W$ [61]. $\hat{X}_{B,i}$ is Bob's received quadrature described by Eq. (22) in Appendix A. If Eve wants to completely hide in the background noise, she can use $W = V_0$. Then Bob will receive the shot-noise level $V(\hat{X}_{B,i}) = V_0$ which is the same as what Alice sent. Although the value of V_0 could be enlarged by frequencies below 1THz, we could gain $V_0 \approx 1$ SNU by cooling down the system to low temperatures.

B. Secret key rate

In this mm-waves and THz CVQKD scheme, Alice and Bob replicate the previous quantum communication protocol several times to generate a string. Then they correct errors in their string by using reconciliation protocol. Direct reconciliation (DR) is the scheme in which Bob uses Alice's encoding string to prepare the key while reverse reconciliation (RR) is when Alice prepares the key based on Bob's decoding result. Alice and Bob use a reconciliation protocol to achieve privacy amplification to reduce the knowledge stole by Eve [68]. In this work, we use an asymptotic secret key rate to study the performance of RR protocol in mm-waves and THz QKD. In RR it is possible to achieve a positive secret key rate when the channel transmissivity is almost 0 while in DR it required a channel transmissivity larger than 0.5 [76], and is impractical in mm-waves and THz because of the high losses (both atmospheric absorption and path).

According to [68], the secret key rate of the MIMO system could be divided into r SISO channels. So we first analyse the secret key rate of a SISO channel. In the RR scheme, Alice and Bob use the decoding outcomes from Bob's side to generate their secret key [74]. Alice and Bob could estimate the mutual information they shared, described as $I(a:b)$, and the accessible information of Eve, described as $I(E:b)$. The asymptotic secret key rate R^∞ could be described by the surplus information shared by Alice and Bob and is given by [62]

$$R^\infty = I(a:b) - I(E:b) \quad (10)$$

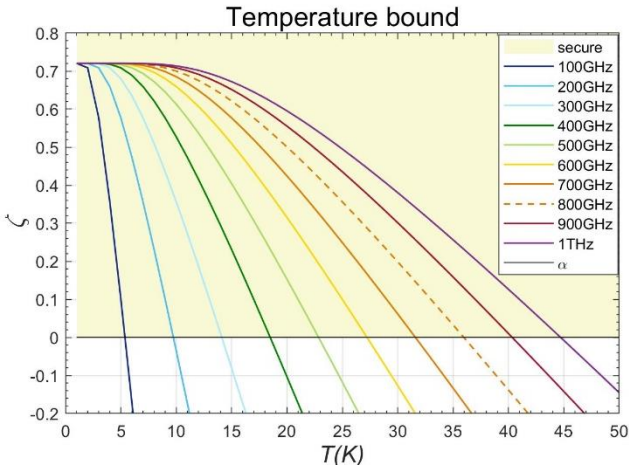


Fig. 2. The curves show ζ as a function of temperature for different frequencies. To achieve secure transmission, ζ should keep above line α (locate in the secure range).

The mutual information between Alice and Bob is

$$I(a:b) = \frac{1}{2} \log_2 \left[1 + \frac{TV_s}{\Lambda(V_0, W)} \right] \quad (11)$$

$$\Lambda(x, y) = Tx + (1 - T)y \quad (12)$$

while $V_s \gg V_0, W$, and Eve's information is bounded by the Holevo information $I(E:b)$ which is defined as

$$I(E:b) = H_E - H_{E|b} \quad (13)$$

where H_E and $H_{E|b}$ are the von Neumann entropy of Eve's total and conditional state given by Eq. (25) and Eq. (26) in Appendix A respectively [68, 75].

The total secret key rate is finally given by the sum of r SISO links' secret key rate [68] assuming $T_i \rightarrow 0$

$$R_{MIMO}^{\leftarrow} = \sum_{i=1}^r R_i^{\leftarrow} \approx \zeta \text{tr}(\mathbf{H}^{\dagger} \mathbf{H}) - rh(W) \quad (14)$$

where

$$\zeta = 0.72 \left[\frac{V_s}{W} - \ln \left(\frac{V_a + 1}{V_a - 1} \right) \left(\frac{V_a^2 - W^2}{2W} - V_a \right) \right] \quad (15)$$

and $\text{tr}(\mathbf{H}^{\dagger} \mathbf{H}) = \sum_{i=1}^r T_i$. $h(W)$ is a function given by

$$h(x) = \frac{x+1}{2} \log_2 \left(\frac{x+1}{2} \right) - \frac{x-1}{2} \log_2 \left(\frac{x-1}{2} \right) \quad (16)$$

C. System conditions

To achieve a positive secret key rate, $\zeta \text{tr}(\mathbf{H}^{\dagger} \mathbf{H}) > rh(W)$ is required. Verified from Eq. (1)-(4), only $\zeta \text{tr}(\mathbf{H}^{\dagger} \mathbf{H})$ in Eq. (14) depends on frequency and ζ also depends on temperature. With a given frequency, lower temperature could decrease V_0 and increase ζ in Eq. (15). This also happens with a given temperature and increasing frequency. But higher frequency normally brings higher path loss which may decrease $\text{tr}(\mathbf{H}^{\dagger} \mathbf{H})$. Since $\text{tr}(\mathbf{H}^{\dagger} \mathbf{H}) > 0$, the limit of $\zeta > \alpha = \frac{rh(W)}{\text{tr}(\mathbf{H}^{\dagger} \mathbf{H})}$ is equal to $\zeta > \alpha = 0$ while $W=1$. This condition helps us find the balance between ζ and $\text{tr}(\mathbf{H}^{\dagger} \mathbf{H})$ and get a positive secret key rate.

Figure 2 shows ζ as a function of temperature for different frequencies in a MIMO THz QKD system [68]. According to the simulation results, we achieved secure transmission for frequencies between $f=100\text{GHz}$ and 1THz , at temperatures $T < 43\text{K}$. The detail of the maximum operating temperature for each

frequency is shown in Table 1.

III. SIMULATION RESULT

We use the secret key rate (R) to define whether the system is safe or not. A positive secret key rate reflects a safe transmission. As R of the MIMO system is the sum of the SISO system, we also compared the different performances of the MIMO and SISO systems at the same conditions.

TABLE I

Frequency	Atmospheric absorption δ	Maximum temperature T_{max} (K)	Distance of 32×32 MIMO system at T_{max} (m)
100GHz	0.4dB/km	4	700
200GHz	3dB/km	8	320
300GHz	4dB/km	13	75
400GHz	20dB/km	17	86
500GHz	50dB/km	21	68
600GHz	150dB/km	26	26
700GHz	70dB/km	30	38
800GHz	100dB/km	35	36
900GHz	100dB/km	39	25
1THz	100dB/km	43	21

A. Simulation of the MIMO system

According to [60], [77], [78], the atmospheric absorption for each frequency is shown in Table 1. We assume the target of the secret key rate is 10^{-5} bit/use [68]. Table 1 also shows the distance of 32×32 MIMO system at maximum temperature for each frequency. While $f=700\text{GHz}$ and $f=800\text{GHz}$ could reach

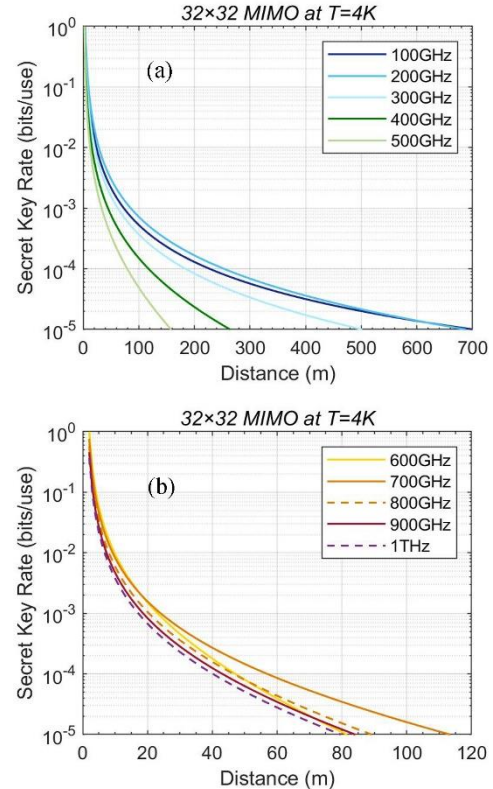


Fig. 3. (a) The transmission distance of a 32×32 MIMO system for $f=100\text{GHz}$ to 500GHz at $T=4\text{K}$. (b) The transmission distance of a 32×32 MIMO system for $f=600\text{GHz}$ to 1THz at $T=4\text{K}$. Here, parameters are $G_a=30$, $W=1$, $V_a=1000$.

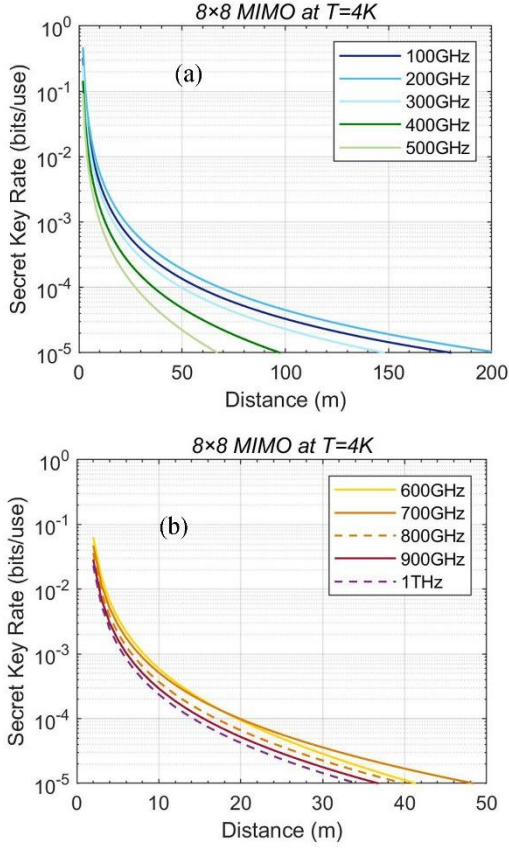


Fig. 4. (a) The transmission distance of an 8×8 MIMO system for $f=100\text{GHz}$ to 500GHz under $T=4K$. (b) The transmission distance of an 8×8 MIMO system for $f=600\text{GHz}$ to 1THz under $T=4K$. Here, parameters are $G_a=30$, $W=1$, $V_a=1000$.

more than 35m at $T>30K$, $f=600\text{GHz}$ could only get to 26m at a lower temperature because of higher absorption at this frequency. Figure 3 shows the secret key rate as a function of secure transmission distance for frequencies from $f=100\text{GHz}$ to 1THz at $T=4K$ in a 32×32 MIMO system. The distance of $f=100\text{GHz}$ and $f=200\text{GHz}$ could achieve $d=700\text{m}$ at $T=4K$ which is the maximum through all frequencies. The secure distance for $f=300\text{GHz}$ could get to $d=500\text{m}$ but it will drop to under $d=160\text{m}$ for frequencies above $f=500\text{GHz}$. If the number

of antennas reduces to 8×8 , the maximum distance could still reach $d=200\text{m}$ for $f=200\text{GHz}$ as shown in Fig. 4 (a). But for frequencies above $f=600\text{GHz}$ in Fig. 4 (b), the distances are all below 50m because of the high absorption.

High MIMO configuration could enhance the maximum secure distance as shown in Fig. 5. While the maximum distance is $d=700\text{m}$ for a 32×32 MIMO system, the secure transmission could achieve much more than $d=8000\text{m}$ for a 1024×1024 MIMO at $f=100\text{GHz}$ at $T=4K$ as shown in Fig. 5 (a). The same trend could be found for $f=200\text{GHz}$ at $T=8K$ and $f=1\text{THz}$ at $T=43K$. For $f=200\text{GHz}$, the maximum distance is more than $d=3000\text{m}$ for 1024×1024 MIMO at $T=8K$. But secure distances for $f=1\text{THz}$ at $T=43K$ are not as much shorter because of the high channel loss caused by atmospheric absorption and thermal noise. It could only get to 160m with a 1024×1024 MIMO antenna system at $T=43K$. And compared with Fig. 3 (b), the distance for $f=1\text{THz}$ at $T=43K$ is just one-fifth of $T=4K$, with 32×32 antennas.

B. Simulation of the SISO system

Compared with a large MIMO scheme, the maximum distance of a SISO scheme is shorter at frequency ranges between $f=100\text{GHz}$ and $f=1\text{THz}$. We assume the target secret key rate is 10^{-5} bit/use [68]. Figure 6 (a) shows that the maximum distance in the SISO system is less than 12m for $f=200\text{GHz}$ at $T=8K$, which is much less than what is observed in a MIMO system shown in Fig. 5 (b). Figure 6 (b) shows the distance for $f=100\text{GHz}$ - 1THz in a SISO scheme at $T=4K$. We could find that the maximum distance decrease with higher frequency at 200GHz - 1THz range caused by the path loss. Comparing Figs. 6 (a) and (b), it is obverse that lower temperature increases the maximum distance for the same frequency.

Comparing Fig. 6 (b) with Fig. 4 we find that at the same temperature, the MIMO scheme could achieve a longer distance than the SISO scheme. So it is necessary to use multiple antennas in mm-waves and THz QKD system. As frequencies $f=800\text{GHz}$, $f=900\text{GHz}$, and $f=1\text{THz}$ have the same atmospheric absorption, Fig. 6 (b) shows that the transmission distance improved by the lower frequency. This may cause by the increase of $\text{tr}(\mathbf{H}^\dagger \mathbf{H})$ as lower frequencies have less free-space path loss and matter more than the increase of V_0 (which in turn

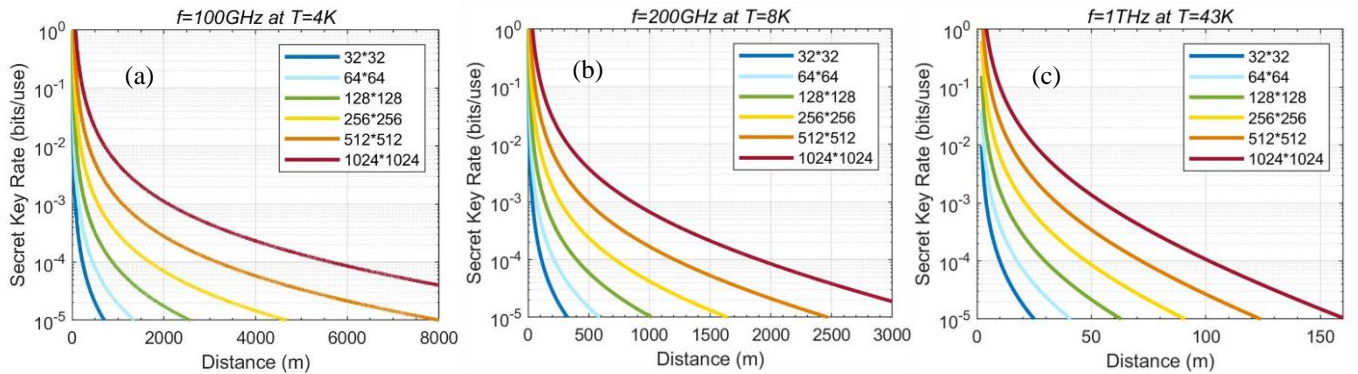


Fig. 5. The curves show the secret key rate as a function of transmission distance for the different numbers of antennas in MIMO systems. (a) is the result for $f=100\text{GHz}$, at $T=4K$. (b) is the result for $f=200\text{GHz}$, at $T=8K$. and (c) is the result for $f=1\text{THz}$, at $T=43K$.

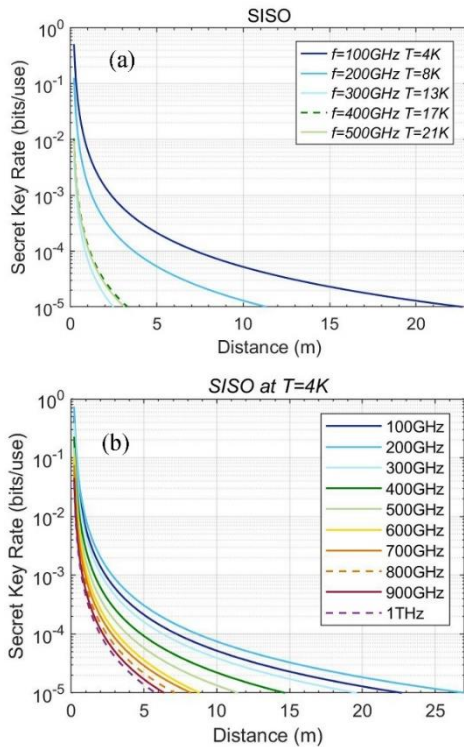


Fig. 6. (a) The secret key rate R as a function of transmission distance for SISO for frequency ranges between $f=100\text{GHz}$ and $f=500\text{GHz}$ at the highest operational temperature. Atmospheric absorptions in the channel are shown in table 1. (b) The secret key rate R as a function of transmission distance for SISO for frequency ranges between $f=100\text{GHz}$ and $f=1\text{THz}$ at $T=4\text{K}$.

decreases ζ) at this range. As a result, to enhance the secure distance, we could use more antennas, cool down the temperature or choose lower frequencies.

IV. CONCLUSION

In this work, we studied the SISO, and MIMO QKD schemes in mm-waves and THz frequency ranges, from $f=0.1$ to $f=1$ THz, with the cryogenic operation of sources and detectors. We found that a positive secret key rate can be observed at the targeted frequency range. MIMO technology could improve the secure transmission distance compared with the SISO scheme. Moreover, we showed that the more antennas are in the system the longer transmission distance could be achieved. To build a long-way secure communication channel, more antennas, low-temperature operation and lower frequencies are required. We assumed the perfect quality of the beam-splitter and communication channel in this study, however, there are still many research efforts to be performed to accomplish the whole scheme in practical hardware.

REFERENCES

[1] T. Nagatsuma *et al.*, "Terahertz wireless communications based on photonics technologies," *Optics Express*, vol. 21, no. 20, pp. 23736-23747, 2013.
 [2] D. M. M. Thomas Kürner, Tadao Nagatsuma, *THz Communications: Paving the Way Towards Wireless Tbps*. Springer ISBN: 978-3-030-73738-2.

[3] K. Delfanzari, R. A. Klemm, H. J. Joyce, D. A. Ritchie, and K. Kadowaki, "Integrated, Portable, Tunable, and Coherent Terahertz Sources and Sensitive Detectors Based on Layered Superconductors," *Proceedings of the IEEE*, vol. 108, no. 5, pp. 721-734, 2020.
 [4] H. Elayan, O. Amin, R. M. Shubair, and M. S. Alouini, "Terahertz communication: The opportunities of wireless technology beyond 5G," in *2018 International Conference on Advanced Communication Technologies and Networking (CommNet)*, 2-4 April 2018 2018, pp. 1-5, doi: 10.1109/COMMNET.2018.8360286.
 [5] K. Kadowaki *et al.*, "Quantum terahertz electronics (QTE) using coherent radiation from high temperature superconducting Bi₂Sr₂CaCu₂O_{8+δ} intrinsic Josephson junctions," *Physica C: Superconductivity*, vol. 491, pp. 2-6, 2013.
 [6] M. J. Fitch and R. Osiander, "Terahertz waves for communications and sensing," *JOHNS HOPKINS APL TECHNICAL DIGEST*, vol. 25, no. 4, pp. 348-355, 2004.
 [7] Z. T. Ma, Z. X. Geng, Z. Y. Fan, J. Liu, and H. D. Chen, "Modulators for Terahertz Communication: The Current State of the Art," *Research*, vol. 2019, 2019.
 [8] Z. Chen *et al.*, "A survey on terahertz communications," *China Communications*, vol. 16, no. 2, pp. 1-35, 2019.
 [9] Z. Chen *et al.*, "Terahertz Wireless Communications for 2030 and Beyond: A Cutting-Edge Frontier," *IEEE Communications Magazine*, vol. 59, no. 11, pp. 66-72, 2021.
 [10] H. Sariieddeen, M. S. Alouini, and T. Y. Al-Naffouri, "An Overview of Signal Processing Techniques for Terahertz Communications," *Proceedings of the IEEE*, vol. 109, no. 10, pp. 1628-1665, 2021.
 [11] H. J. Song and T. Nagatsuma, "Present and Future of Terahertz Communications," *IEEE Transactions on Terahertz Science and Technology*, vol. 1, no. 1, pp. 256-263, 2011.
 [12] M. Tsujimoto *et al.*, "Broadly Tunable Subterahertz Emission from Internal Branches of the Current-Voltage Characteristics of Superconducting Bi₂Sr₂CaCu₂O_{8+δ} Single Crystals," *Physical Review Letters*, vol. 108, no. 10, 2012.
 [13] K. Delfanzari *et al.*, "Terahertz Oscillating Devices Based Upon the Intrinsic Josephson Junctions in a High Temperature Superconductor," *Journal of Infrared Millimeter and Terahertz Waves*, vol. 35, no. 1, pp. 131-146, 2014.
 [14] I. F. Akyildiz, C. Han, Z. Hu, S. Nie, and J. M. Jornet, "Terahertz Band Communication: An Old Problem Revisited and Research Directions for the Next Decade," *IEEE Transactions on Communications*, vol. 70, no. 6, pp. 4250-4285, 2022.
 [15] K. Delfanzari *et al.*, "Experimental and Theoretical Studies of Mesas of Several Geometries for Terahertz Wave Radiation from the Intrinsic Josephson Junctions in Superconducting Bi₂Sr₂CaCu₂O_{8+δ}" in *37th International Conference on Infrared, Millimeter, and Terahertz Waves (IRMMW-THz)*, Univ Wollongong, Wollongong, AUSTRALIA, Sep 23-28 2012, in International Conference on Infrared Millimeter and Terahertz Waves, 2012.
 [16] R. H. Caverly, "Breakthroughs in Microwaves: Programmable Terahertz Chip-Scale Surfaces and Systems—An Interview With Dr. Kaushik Sengupta," *IEEE Journal of Microwaves*, vol. 1, no. 4, pp. 853-863, 2021.
 [17] K. Delfanzari *et al.*, "Tunable terahertz emission from the intrinsic Josephson junctions in acute isosceles triangular Bi₂Sr₂CaCu₂O_{8+δ} mesas," *Optics Express*, vol. 21, no. 2, pp. 2171-2184, 2013.
 [18] T. Kashiwagi *et al.*, "High Temperature Superconductor Terahertz Emitters: Fundamental Physics and Its Applications," *Japanese Journal of Applied Physics*, vol. 51, no. 1, 2012.
 [19] T. Kashiwagi *et al.*, "Efficient Fabrication of Intrinsic-Josephson-Junction Terahertz Oscillators with Greatly Reduced Self-Heating Effects," *Physical Review Applied*, vol. 4, no. 5, 2015.
 [20] T. Kashiwagi *et al.*, "Study of Radiation Characteristics of Intrinsic Josephson Junction Terahertz Emitters with Different Thickness of Bi₂Sr₂CaCu₂O_{8+δ} Crystals," *Materials*, vol. 14, no. 5, doi: 10.3390/ma14051135.
 [21] K. Delfanzari *et al.*, "Effect of Bias Electrode Position on Terahertz Radiation From Pentagonal Mesas of Superconducting Bi₂Sr₂CaCu₂O_{8+δ}," *IEEE Transactions on Terahertz Science and Technology*, vol. 5, no. 3, pp. 505-511, 2015.
 [22] Y. Xiong, T. Kashiwagi, R. A. Klemm, K. Kadowaki, and K. Delfanzari, "Engineering the Cavity modes and Polarization in Integrated Superconducting Coherent Terahertz Emitters," in *2020*

- 45th International Conference on Infrared, Millimeter, and Terahertz Waves (IRMMW-THz), 8-13 Nov. 2020 2020, pp. 1-2, doi: 10.1109/IRMMW-THz46771.2020.9370587.
- [23] K. Delfanzari *et al.*, "Study of coherent and continuous terahertz wave emission in equilateral triangular mesas of superconducting $\text{Bi}_2\text{Sr}_2\text{CaCu}_2\text{O}_{8+\delta}$ intrinsic Josephson junctions," *Physica C-Superconductivity and Its Applications*, vol. 491, pp. 16-19, 2013.
- [24] Y. Saiwai *et al.*, "Liquid helium-free high-Tc superconducting terahertz emission system and its applications," *Japanese Journal of Applied Physics*, vol. 59, no. 10, p. 105004, 2020.
- [25] K. A. Fedorova *et al.*, "Widely Tunable Terahertz-Generating Semiconductor Disk Laser," *physica status solidi (RRL) – Rapid Research Letters*, vol. 14, no. 10, p. 2000204, 2020.
- [26] R. Cattaneo, E. A. Borodianskyi, A. A. Kalenyuk, and V. M. Krasnov, "Superconducting Terahertz Sources with 12% Power Efficiency," *Physical Review Applied*, vol. 16, no. 6, 2021.
- [27] J. R. Rain *et al.*, "Wave functions for high-symmetry, thin microstrip antennas, and two-dimensional quantum boxes," *Physical Review A*, vol. 104, no. 6, p. 062205, 2021.
- [28] Y. Xiong and K. Delfanzari, "Engineering Circular Polarization in Chip-integrated High-Tc Superconducting THz Antennas," in *2021 Photonics & Electromagnetics Research Symposium (PIERS)*, 21-25 Nov. 2021 2021, pp. 1016-1019, doi: 10.1109/PIERS53385.2021.9694960.
- [29] Y. Xie, N. Bai, W. Hong, and X. Sun, "Study of a hexagonal lattice defect photonic crystal waveguide slow wave structure for G-band traveling wave tube," *Journal of Electromagnetic Waves and Applications*, vol. 36, no. 6, pp. 843-855, 2022.
- [30] D. P. Cerkoney *et al.*, "Cavity mode enhancement of terahertz emission from equilateral triangular microstrip antennas of the high-Tc superconductor $\text{Bi}_2\text{Sr}_2\text{CaCu}_2\text{O}_{8+\delta}$," *Journal of Physics: Condensed Matter*, vol. 29, no. 1, p. 015601, 2017.
- [31] R. A. Klemm *et al.*, "Modeling the electromagnetic cavity mode contributions to the THz emission from triangular $\text{Bi}_2\text{Sr}_2\text{CaCu}_2\text{O}_{8+\delta}$ mesas," *Physica C: Superconductivity*, vol. 491, pp. 30-34, 2013.
- [32] S. Kalhor, M. Ghanaatshoar, and K. Delfanzari, "On-chip Superconducting THz Metamaterial Bandpass Filter," in *2020 45th International Conference on Infrared, Millimeter, and Terahertz Waves (IRMMW-THz)*, 8-13 Nov. 2020 2020, pp. 1-2, doi: 10.1109/IRMMW-THz46771.2020.9370663.
- [33] K. Yang, S. Liu, S. Arezoomandan, A. Nahata, and B. Sensale-Rodriguez, "Graphene-based tunable metamaterial terahertz filters," *Applied Physics Letters*, vol. 105, no. 9, p. 093105, 2014.
- [34] I. J. H. McCrindle, J. Grant, T. D. Drysdale, and D. R. S. Cumming, "Multi-Spectral Materials: Hybridisation of Optical Plasmonic Filters and a Terahertz Metamaterial Absorber," *Advanced Optical Materials*, vol. 2, no. 2, pp. 149-153, 2014.
- [35] S. Kalhor, M. Ghanaatshoar, H. J. Joyce, D. A. Ritchie, K. Kadowaki, and K. Delfanzari, "Millimeter-Wave-to-Terahertz Superconducting Plasmonic Waveguides for Integrated Nanophotonics at Cryogenic Temperatures," *Materials*, vol. 14, no. 15, 2021.
- [36] S. Atakaramians, S. Afshar V, T. M. Monro, and D. Abbott, "Terahertz dielectric waveguides," *Advances in Optics and Photonics*, vol. 5, no. 2, pp. 169-215, 2013.
- [37] S. Kalhor, M. Ghanaatshoar, and K. Delfanzari, "Guiding of terahertz photons in superconducting nano-circuits," in *2020 International Conference on UK-China Emerging Technologies (UCET)*, 20-21 Aug. 2020 2020, pp. 1-3, doi: 10.1109/UCET51115.2020.9205480.
- [38] G. Gallot, S. P. Jamison, R. W. McGowan, and D. Grischkowsky, "Terahertz waveguides," *J. Opt. Soc. Am. B*, vol. 17, no. 5, pp. 851-863, 2000.
- [39] K. Wang and D. M. Mittleman, "Metal wires for terahertz wave guiding," *Nature*, vol. 432, no. 7015, pp. 376-379, 2004.
- [40] S. Kalhor, M. Ghanaatshoar, T. Kashiwagi, K. Kadowaki, M. J. Kelly, and K. Delfanzari, "Thermal Tuning of High-Tc Superconducting $\text{Bi}_2\text{Sr}_2\text{CaCu}_2\text{O}_{8+\delta}$ Terahertz Metamaterial," *IEEE Photonics Journal*, vol. 9, no. 5, 2017.
- [41] R. Degl'Innocenti, H. Lin, and M. Navarro-Cía, "Recent progress in terahertz metamaterial modulators," vol. 11, no. 8, pp. 1485-1514, 2022.
- [42] V. Savinov, K. Delfanzari, V. A. Fedotov, and N. I. Zheludev, "Giant nonlinearity in a superconducting sub-terahertz metamaterial," *Applied Physics Letters*, vol. 108, no. 10, p. 101107, 2016.
- [43] A. S. Malishevskii and S. A. Uryupin, "On Cherenkov excitation of electromagnetic waves by vortex travelling in Josephson sandwich," *Physica Scripta*, vol. 97, no. 5, p. 055817, 2022.
- [44] S. Kalhor *et al.*, "Active Terahertz Modulator and Slow Light Metamaterial Devices with Hybrid Graphene-Superconductor Photonic Integrated Circuits," *Nanomaterials*, vol. 11, no. 11, 2021.
- [45] A. Squires, X. Gao, T. van der Laan, Z. Han, and J. Du, "Adding a Tuneable Response to a Terahertz Metasurface Using a Graphene Thin Film," *Journal of Infrared, Millimeter, and Terahertz Waves*, vol. 43, no. 9, pp. 806-818, 2022.
- [46] S. Kalhor *et al.*, "Active Terahertz Modulator and Slow Light Metamaterial Devices with Hybrid Graphene-superconductor Coupled Split-ring Resonator Arrays," in *2022 Photonics & Electromagnetics Research Symposium (PIERS)*, 25-29 April 2022, pp. 967-971, doi: 10.1109/PIERS55526.2022.9792980.
- [47] S. J. Kindness *et al.*, "A Terahertz Chiral Metamaterial Modulator," *Advanced Optical Materials*, vol. 8, no. 21, p. 2000581, 2020.
- [48] C. Li *et al.*, "Electrically terahertz switchable device based on superconducting composite structure metamaterial," *Applied Physics Letters*, vol. 121, no. 3, p. 031702, 2022.
- [49] S. J. Kindness *et al.*, "Graphene-Integrated Metamaterial Device for All-Electrical Polarization Control of Terahertz Quantum Cascade Lasers," *ACS Photonics*, vol. 6, no. 6, pp. 1547-1555, 2019.
- [50] F. Sizov and A. Rogalski, "THz detectors," *Progress in Quantum Electronics*, vol. 34, no. 5, pp. 278-347, 2010.
- [51] S. Castilla *et al.*, "Fast and Sensitive Terahertz Detection Using an Antenna-Integrated Graphene pn Junction," *Nano Letters*, vol. 19, no. 5, pp. 2765-2773, 2019.
- [52] R. A. Lewis, "A review of terahertz detectors," *Journal of Physics D: Applied Physics*, vol. 52, no. 43, p. 433001, 2019.
- [53] M. Zhang, Foshat, P., Poorgholam Khanjari, S., Imran, M., Weides, M. and Delfanzari, K., "Microwave Quantum Key Distribution with Cryogenic Microwave Components for Superconducting Quantum Computing," presented at the 2022 International Symposium on Quantum Computing: Circuits Systems Automation and Applications (QC-CSAA), Knoxville, TN, USA, 18-19 July 2022.
- [54] P. Magnard *et al.*, "Microwave Quantum Link between Superconducting Circuits Housed in Spatially Separated Cryogenic Systems," *Physical Review Letters*, vol. 125, no. 26, p. 260502, 2020.
- [55] F. K. Florian Fesquet, Michael Renger, Qiming Chen, Kedar Honasoge, Oscar Gargiulo, Yuki Nojiri, Achim Marx, Frank Deppe, Rudolf Gross, Kirill G. Fedorov, "Perspectives of microwave quantum key distribution in open-air," *arXiv:2203.05530*.
- [56] Y. H. Yang, M. Mandehgar, and D. R. Grischkowsky, "Broadband THz Signals Propagate Through Dense Fog," *IEEE Photonics Technology Letters*, vol. 27, no. 4, pp. 383-386, 2015.
- [57] M. Karmoose, C. Fragouli, S. Diggavi, R. Misoczki, L. L. Yang, and Z. L. Zhang, "Using mm-Waves for Secret Key Establishment," *IEEE Communications Letters*, vol. 23, no. 6, pp. 1077-1080, 2019.
- [58] Z. Q. Wang, R. Malaney, and J. Green, "Inter-satellite Quantum Key Distribution at Terahertz Frequencies," in *IEEE International Conference on Communications (IEEE ICC)*, Shanghai, PEOPLES R CHINA, May 20-24 2019, in IEEE International Conference on Communications, 2019.
- [59] Y. Q. He, Y. Y. Mao, D. Huang, Q. Liao, and Y. Guo, "Indoor channel modeling for continuous variable quantum key distribution in the terahertz band," *Optics Express*, vol. 28, no. 22, pp. 32386-32402, 2020.
- [60] T. Schneider, A. Wiatrek, S. Preussler, M. Grigat, and R. P. Braun, "Link Budget Analysis for Terahertz Fixed Wireless Links," *IEEE Transactions on Terahertz Science and Technology*, vol. 2, no. 2, pp. 250-256, 2012.
- [61] C. Ottaviani *et al.*, "Terahertz Quantum Cryptography," *IEEE Journal on Selected Areas in Communications*, vol. 38, no. 3, pp. 483-495, 2020.
- [62] S. Pirandola *et al.*, "Advances in quantum cryptography," *Advances in Optics and Photonics*, vol. 12, no. 4, pp. 1012-1236, 2020.
- [63] S. Pirandola, R. Laurenza, C. Ottaviani, and L. Banchi, "Fundamental limits of repeaterless quantum communications," *Nature Communications*, vol. 8, 2017.
- [64] S. Pirandola, "Composable security for continuous variable quantum key distribution: Trust levels and practical key rates in

- wired and wireless networks," *Physical Review Research*, vol. 3, no. 4, p. 043014, 2021.
- [65] I. H. L. Grande, S. Etcheverry, J. Aldama, S. Ghasemi, D. Nolan, and V. Pruneri, "Adaptable transmitter for discrete and continuous variable quantum key distribution," *Optics Express*, vol. 29, no. 10, pp. 14815-14827, 2021.
- [66] C. J. Liu, C. H. Zhu, X. Liu, M. Nie, H. Yang, and C. X. Pei, "Multicarrier Multiplexing Continuous-Variable Quantum Key Distribution at Terahertz Bands Under Indoor Environment and in Inter-Satellite Links Communication," *IEEE Photonics Journal*, vol. 13, no. 4, 2021.
- [67] R. H. Shi, J. J. Shi, Y. Guo, X. Q. Peng, and M. H. Lee, "Quantum MIMO Communication Scheme Based on Quantum Teleportation with Triplet States," *International Journal of Theoretical Physics*, vol. 50, no. 8, pp. 2334-2346, 2011.
- [68] N. K. Kundu, S. P. Dash, M. R. McKay, and R. K. Mallik, "MIMO Terahertz Quantum Key Distribution," *IEEE Communications Letters*, vol. 25, no. 10, pp. 3345-3349, 2021.
- [69] R. Jantti, R. Di Candia, R. F. Duan, and K. Ruttik, "Multiantenna Quantum Backscatter Communications," in *36th IEEE Global Communications Conference (GLOBECOM)*, Singapore, SINGAPORE, Dec 04-08 2017, in IEEE Globecom Workshops, 2017.
- [70] H. Deng and A. Sayeed, "Mm-Wave MIMO Channel Modeling and User Localization Using Sparse Beamspace Signatures," in *IEEE 15th International Workshop on Signal Processing Advances in Wireless Communications (SPAWC)*, Toronto, CANADA, Jun 22-25 2014, in IEEE International Workshop on Signal Processing Advances in Wireless Communications, 2014, pp. 130-134.
- [71] S. A. Busari, K. M. S. Huq, S. Mumtaz, and J. Rodriguez, "Terahertz Massive MIMO for Beyond-5G Wireless Communication," in *IEEE International Conference on Communications (IEEE ICC)*, Shanghai, PEOPLES R CHINA, May 20-24 2019, in IEEE International Conference on Communications, 2019.
- [72] B. Kraus, N. Gisin, and R. Renner, "Lower and Upper Bounds on the Secret-Key Rate for Quantum Key Distribution Protocols Using One-Way Classical Communication," *Physical Review Letters*, vol. 95, no. 8, p. 080501, 2005.
- [73] R. Renner and J. I. Cirac, "de Finetti Representation Theorem for Infinite-Dimensional Quantum Systems and Applications to Quantum Cryptography," *Physical Review Letters*, vol. 102, no. 11, p. 110504, 2009.
- [74] F. Grosshans, G. Van Assche, J. Wenger, R. Brouri, N. J. Cerf, and P. Grangier, "Quantum key distribution using gaussian-modulated coherent states," *Nature*, vol. 421, no. 6920, pp. 238-241, 2003.
- [75] C. Weedbrook *et al.*, "Gaussian quantum information," *Reviews of Modern Physics*, vol. 84, no. 2, pp. 621-669, 2012.
- [76] C. Weedbrook, S. Pirandola, S. Lloyd, and T. C. Ralph, "Quantum Cryptography Approaching the Classical Limit," *Physical Review Letters*, vol. 105, no. 11, 2010.
- [77] J. Y. Sun, F. J. Hu, and S. Lucyszyn, "Predicting Atmospheric Attenuation Under Pristine Conditions Between 0.1 and 100 THz," *IEEE Access*, vol. 4, pp. 9377-9399, 2016.
- [78] Y. H. Yang, A. Shutler, and D. Grischkowsky, "Measurement of the transmission of the atmosphere from 0.2 to 2 THz," *Optics Express*, vol. 19, no. 9, pp. 8830-8838, 2011.

APPENDIX A

A. Computation of channel model

The channel matrix between Alice and Bob could be modelled as Eq. (4)

$$\mathbf{H} = \sum_{l=1}^L \sqrt{\gamma_l} e^{j2\pi f_c \tau_l} \psi_{N_r}(\phi_{r,LOS}) \psi_{N_t}^\dagger(\phi_{t,LOS})$$

where, $\mathbf{H} \in \mathbb{C}^{N_r \times N_t}$, L is the full number of multipath components, τ_l is the propagation delay of the l -th multipath. The path loss γ_l for the line-of-sight (LOS) path ($L=1$) is given by Eq. (5)

$$\gamma_{l=1} = G_t G_r \left(\frac{\lambda}{4\pi d} \right)^2 10^{-\frac{\delta d}{10}}$$

where d is the distance (km) between Alice and Bob and δ is the atmospheric loss. $\phi_{r,LOS}$ and $\phi_{t,LOS}$ is the angle of arrival seen by Bob, and the angle of departure from Alice, respectively. $\psi_K(\theta)$ represents the array response vector of a ULA which contains K number of antennas [68]:

$$\psi_K(\theta) = \frac{1}{\sqrt{K}} \left[1, e^{j2\pi \frac{d_a}{\lambda} \sin\theta}, \dots, e^{j2\pi \frac{d_a}{\lambda} (K-1) \sin\theta} \right]^T \quad (17)$$

Here, d_a and λ denote the inter-antenna spacing and wavelength of the carrier signal, respectively. We assume $d_a = \frac{\lambda}{4}$ in this work. The channel model could be described by a singular-value decomposition (SVD) scheme introduced by Ref. [68]:

$$\mathbf{H} = \mathbf{U} \mathbf{\Sigma} \mathbf{V}^\dagger \quad (18)$$

Here, $\mathbf{U} \in \mathbb{C}^{N_r \times N_r}$ and $\mathbf{V} \in \mathbb{C}^{N_t \times N_t}$ are unitary matrices represent K phase shifters [69], and $\mathbf{\Sigma}$ is given as

$$\mathbf{\Sigma} = \begin{bmatrix} \text{diag}\{\sqrt{\eta_1}, \dots, \sqrt{\eta_r}\} & \mathbf{0}_{r \times (N_t-r)} \\ \mathbf{0}_{(N_r-r) \times r} & \mathbf{0}_{(N_r-r) \times (N_t-r)} \end{bmatrix} \quad (19)$$

where r is the rank of \mathbf{H} and $\sqrt{\eta_1}, \dots, \sqrt{\eta_r}$ are the r non-zero singular values of \mathbf{H} generated by the transmissivity of beam-splitters in the system [69].

As shown in Fig.1 (b), the whole model of a MIMO system could be described by [68, 69]

$$\hat{\mathbf{a}}_B = \mathbf{U}^\dagger \mathbf{H} \mathbf{V} \hat{\mathbf{a}}_A + \mathbf{U}^\dagger \mathbf{U} \mathbf{S} \hat{\mathbf{a}}_E \quad (20)$$

where $\hat{\mathbf{a}}_B = [\hat{a}_{B,1}, \dots, \hat{a}_{B,N_r}]^T$ is the received mode of Bob, $\hat{\mathbf{a}}_A = [\hat{a}_{A,1}, \dots, \hat{a}_{A,N_t}]^T$ is the transmitted mode of Alice, $\hat{\mathbf{a}}_E = [\hat{a}_{E,1}, \dots, \hat{a}_{E,N_t}]^T$ is the injected Gaussian mode of Eve.

$$\mathbf{S} = \text{diag}\{\sqrt{1-\eta_1}, \dots, \sqrt{1-\eta_r}, \mathbf{1}_{(M-r) \times 1}\} \quad (21)$$

is a diagonal matrix with $M = \min(N_t, N_r)$. We get $\mathbf{U}^\dagger \mathbf{U} = \mathbf{I}_{N_r}$ and $\mathbf{V}^\dagger \mathbf{V} = \mathbf{I}_{N_t}$ as \mathbf{U} and \mathbf{V} are unitary matrices. Considering Eq. (18) $\mathbf{H} = \mathbf{U} \mathbf{\Sigma} \mathbf{V}^\dagger$, diagonal matrix $\mathbf{\Sigma}$ and \mathbf{S} , Eq. (20) would turn to $\hat{\mathbf{a}}_B = \mathbf{U}^\dagger \mathbf{U} \mathbf{\Sigma} \mathbf{V}^\dagger \mathbf{V} \hat{\mathbf{a}}_A + \mathbf{U}^\dagger \mathbf{U} \mathbf{S} \hat{\mathbf{a}}_E = \mathbf{\Sigma} \hat{\mathbf{a}}_A + \mathbf{S} \hat{\mathbf{a}}_E$. So the efficient channel between Alice and Bob can be disintegrated into r parallel SISO channels.

Bob randomly chooses quadratures for his input and operates homodyne measurements. Then the input-output relationship of i -th parallel channel between Bob's received quadrature $\hat{X}_{B,i}$, and Alice's transmitted quadrature $\hat{X}_{A,i}$, can be written by a generic quantum channel as [68]

$$\hat{X}_{B,i} = \sqrt{T_i} \hat{X}_{A,i} + \sqrt{1-T_i} \hat{X}_{E,i}, \quad i = 1, 2, \dots, r \quad (22)$$

with T_i and $\hat{X}_{E,i}$ as transmittance, and Eve's excess noise quadrature, respectively. We can write for Eve's ancilla mode:

$$\hat{X}_{E,i} = -\sqrt{1-T_i} \hat{X}_{A,i} + \sqrt{T_i} \hat{X}_{E,i}, \quad i = 1, 2, \dots, r \quad (23)$$

B. Computation of the secret key rate

The secret key rate $R^\leftarrow = I(a:b) - I(E:b)$ is given defined by mutual information. Assuming Gaussian statistic for simulating purposes, the mutual information between Alice and Bob is

$$I(a:b) = \frac{1}{2} \log_2 \left[1 + \frac{TV_s}{\Lambda(V_0, W)} \right]$$

$$\Lambda(x, y) = Tx + (1-T)y$$

And Eve's information is bounded by the Holevo information $I(E:b)$ which is defined as

$$I(E: b) = H_E - H_{E|b} \quad (24)$$

$$H_E = h(v_1) + h(v_2) \quad (25)$$

$$H_{E|b} = h(v_3) + h(v_4) \quad (26)$$

where H_E and $H_{E|b}$ are the von Neumann entropy of Eve's total and conditional state respectively [68, 75]. The von Neumann entropy depends on symplectic eigenvalues is given by [68]

$$v_1 = \Lambda(W, V_a), v_2 = W, \quad (27)$$

$$v_3, v_4 = \sqrt{\frac{1}{2}(\Delta \pm \sqrt{\Delta^2 - 4Y})}, \quad (28)$$

and

$$\Delta = \frac{V_a W \Lambda(W, V_a) + W \Lambda(W V_a, 1)}{\Lambda(V_a, W)} \quad (29)$$

$$Y = \frac{V_a W^2 \Lambda(W, V_a) \Lambda(W V_a, 1)}{\Lambda^2(V_a, W)} \quad (30)$$

The function $h(x)$ is defined as

$$h(x) = \frac{x+1}{2} \log_2 \left(\frac{x+1}{2} \right) - \frac{x-1}{2} \log_2 \left(\frac{x-1}{2} \right) \quad (31)$$